COMPUTER SIMULATION OF BRITTLE CRACK PROPAGATION AND ARREST OF STEEL PLATE WITH TEMPERATURE GRADIENT BASED ON LOCAL FRACTURE STRESS CRITERION

Susumu Machida[1], Hitoshi Yoshinari[1], and Shuji Aihara[2]

1 Department of Naval Architecture and Ocean Engineering, The Univeristy of Tokyo.
2 Nagoya R&D Laboratories, Nippon Steel Corporation.

ABSTRACT: A fracture mechanical model for brittle crack propagation and arrest is proposed based on the local fracture stress criterion. Dynamic fracture toughness (K_D) for a propagating crack is calculated as a function of crack velocity and temperature. The model is extended to incorporate the effect of unbroken ligament (UL) formed near the plate surfaces and crack-front-bowing. The model simulates acceleration, deceleration and arrest of a crack in a ESSO or a double-tension test plate with temperature-gradient. Calculated arrested crack lengths compare well with experimental results. It is shown that the conventional crack arrest toughness calculated from applied stress and arrested crack length depends on temperature-gradient but not a unique material property.

KEYWORDS: dynamic fracture, stress intensity factor, arrest toughness, shear lip, crack velocity.

INTRODUCTION

The concept of crack arrestability has been successfully applied to such welded steel structures as ships and storage tanks for ensuring safety against catastrophic failure by brittle crack propagation. The crack arrest toughness, K_{ca}, is measured by using double tension test or ESSO test with temperature-gradient in the specimen[1]. Value of K_{ca} is compared with stress intensity factor, K, which is calculated from applied stress and possible maximum length of a propagating crack in the structure considered. If K_{ca} is greater than K, then crack arrest is ensured. Alternatively, K_{ca} value required for steel is determined so that K_{ca} is greater than K. Because above criterion is based on the static approximation, it might possibly fail to predict the actual crack arrest behavior. The behavior of brittle crack propagation and arrest is far from complete understanding.

The brittle crack propagation is intrinsically dynamic. The dynamic effect is two fold; one is a mechanical effect, simply expressed as inertial effect, and the other is a material response to high strain rate, especially strain rate dependence of yielding behavior [2]. The latter is especially important for ferritic steels because their yield stress depends on strain rate strongly. Moreover, a propagating crack accompanies shear-lips near plate surfaces. In addition, the propagating crack front is not straight but bows in the middle of the plate thickness; there exist a distribution of K and crack velocity normal to the crack front. All these factors have influences on the crack propagation and arrest behavior.

Kanazawa et al. [1] showed that K_{ca} values obtained from the standard size (W=0.5m) double tension tests and that from very wide (W=2.0m) duplex-type ESSO tests did not coincide. The reason of the discrepancy was presumed to be a lack of dynamic consideration. They conducted dynamic elastic analyses using FDM and obtained dynamic fracture toughness as a function of crack velocity and temperature based on the energy balance concept. In spite of their fully dynamic analyses, the experimental crack propagation and arrest behavior was not completely explained. Importance of the influence of the shear-lips was pointed out.

They also noted that the energy criterion is only a *necessary* condition and local criterion is necessary.

The authors proposed a fundamental crack propagation model based on the local fracture stress criterion [3]. First in the present paper, the model is outlined, and then it is extended to simulate the crack propagation and arrest behavior in a specimen with temperature-gradient (extended model). Factors influencing K_{ca} are discussed based on the model.

FUNDAMENTAL MODEL (DETERMINATION OF DYNAMIC FRACTURE TOUGHNESS)

Theory

Brittle-cleavage fracture initiation of steel is stress-controlled. Transition behavior of cleavage initiation toughness, K_c or K_{IC}, can be predicted from local fracture stress, σ_F, and temperature dependence of yield stress (the RKR model [4]). σ_F is a parameter which is insensitive to temperature and stress triaxiality [5]. It

is presumed that σ_F is insensitive to strain rate and a local fracture model similar to the RKR model can be applied to a crack propagating dynamically in a brittle-cleavage manner in steel. We assume that a crack continues to propagate with tensile stress ahead of the crack-tip exceeding σ_F within a characteristic distance, r_c, see Fig.1.

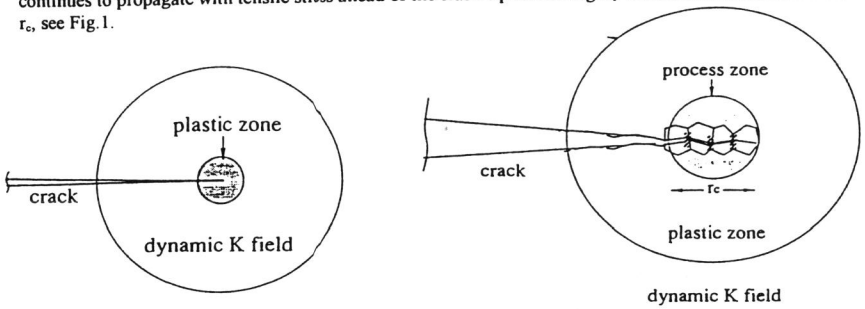

Fig.1—Deformation and stress field around a propagationg crack-tip.

$$\sigma_{yy}[r_c, 0] = \sigma_F \tag{1}$$

where, $\sigma_{ij}[r,\theta]$ is stress component, (r, θ) is polar coordinate with origin at the crack-tip and $\theta = 0$ for crack advancing direction.

A complete solution for stress field around a dynamically propagation crack-tip in elastic-plastic solid has not been available yet. Achenbach et al. [6] obtained an asymptotic solution for elastic and linear strain-hardening solid. Their solution does not give absolute stress values but gives a stress singularity and relative stress distribution in a circumferential direction as a function of crack velocity and tangent modulus, E_t. They also found that upper limit crack velocity coincides with the Rayleigh wave speed calculated using E_t, instead of Young's modulus, E. Referring to the HRR field for a stationary crack [7], it is assumed that the stress field for a dynamically propagating crack is expressed by,

$$\sigma_{ij}[r, \theta] = \sigma_Y \left\{ (1 - \nu^2) \left(\frac{K_d}{\sigma_Y} \right)^2 \frac{1}{r} \right\}^{-s} \Sigma_{ij}[\theta, V] \tag{2}$$

where K_d is dynamic stress intensity factor, ν is Poisson's ratio, σ_Y is yield stress, $\Sigma_{ij}[\theta,V]$ is a non-dimensional function of θ and V and nearly equal to 4 for $V/c_R<0.5$ under plane-strain condition, V is crack velocity, c_R is elastic Rayleigh wave speed and "s" is a stress singularity parameter. Achenbach et al. [6]

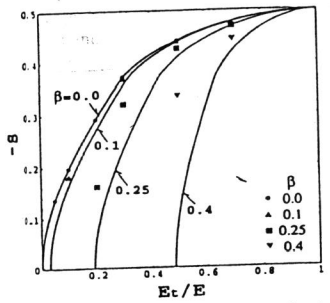

Fig.2—Stress singularity exponent based on Achenbach's model.

calculated "s" as shown in the plots in Fig.2, $\alpha = E_t/E$, and β is crack velocity normalized by the bar-wave velocity, $b = V/(E/\rho)^{1/2}$, ρ is density of solid. It is noted that the stress singularity vanishes at $b = 0.57\,\alpha^{1/2}$ and there is no solution beyond that velocity. It is assumed that "s" is simply expressed by,

$$s[\alpha, \beta] = s_{\beta=0}\left[\frac{\alpha - (\beta / 0.57)^2}{1 - (\beta / 0.57)^2} \right] \tag{3}$$

where $s_{\beta=0}[.]$ is the stress singularity for a crack growing quasi-statically in elastic and linear strain-hardening solid [8]. Lines in Fig.2 are graphical expressions of Eq.(3).

Strain-hardening behavior of most metals is better approximated by power-hardening law ($e_e = \sigma_Y/E$ $(\sigma_e / \sigma_Y)^n$, for $\sigma_e > \sigma_Y$) and instantaneous hardening rate depends on equivalent strain e_e, or equivalent stress, σ_e. Instantaneous tangent modulus is expressed by,

$$E_t = \frac{d\sigma_e}{d\varepsilon_e} = \frac{1}{n} E \left(\frac{\sigma_e}{\sigma_Y} \right)^{-(n-1)} \tag{4}$$

where n is reciprocal of strain-hardening exponent, is applied to Eq.(3). Analogously to Eq.(2), σ_e in Eq.(4) is expressed by,

$$\sigma_e[r, \theta] = \sigma_Y \left\{ (1 - \nu^2) \left(\frac{K_d}{\sigma_Y} \right)^2 \frac{1}{r} \right\}^{-s} \Sigma_e[\theta, V] \tag{5}$$

where $\Sigma_e[\theta,V]$ is a non-dimensional function of θ and V and equal to unity for $\theta = 0$. It should be noted here that Eq.(4) is evaluated at $r=r_c$. Equation (2) is based on a constant E_t throughout the plastic zone. However, in a power-hardening material, instantaneous tangent modulus changes with "r". Strictly, varying E_t cannot be applied in Eqs.(2) and (3). However, our concern is the stress level at $r=r_c$ not only stress distribution but throughout the plastic zone. In this sense, application of Eq.(4) seems to be a reasonable approximation.

As noted earlier, yield stress of steel depends strongly on strain-rate, e. Dependence of yield stress on e and temperature is expressed as a sum of thermally activated and phonon drag components [9]. The following expression is used.

$$\sigma_Y = \sigma_{Y0} + (9.0 \times 10^{-4}) T_0 E \left(\frac{\sigma_{Y0}}{E} \right)^{-1/2} \times \left\{ \frac{1}{T \ln[10^8 / \dot{\varepsilon}_e]} - \frac{1}{T_0 \ln[10^8 / \dot{\varepsilon}_{e0}]} \right\} + \eta \dot{\varepsilon}_e \tag{6}$$

where, T is temperature in Kelvin, $T_0=293K$, $e_{e0}=10^{-4}s^{-1}$, σ_{Y0} is yield stress at T_0 and e_{e0}. We use a value $\eta=2.0 \times 10^{-3}$MPa.s in the phonon drag term determined experimentally for mild steel [10]. This term is especially important at high strain-rate encountered in the plastic zone of a propagating crack-tip.

Assuming a steady state crack propagation, e_e is expressed as,

$$e_e = \frac{\dot{\sigma}_e}{E_t} = -\frac{\sigma_Y}{E_t} V \quad s \left\{ (1 - \nu)^2 \left(\frac{K_d}{\sigma_Y} \right) \frac{1}{r} \right\}^{-s} \times r^{-1} \Sigma_e[\theta, V] \tag{7}$$

Eq.(7) is applied at $r=r_c$.

Inserting Eq.(2) into Eq.(1), inserting Eq.(5) into Eq.(4), and rewriting Eq.(7), we obtain three simultaneous equations. In these equations, σ_Y is expressed by Eq.(6). Unknown parameters are e_e, a, V and K_d. If any one of them is given, other parameters are determined by solving the non-linear equations simultaneously. Value of K_d determined in this manner is the dynamic fracture toughness and denoted K_D. K_D is expressed as a function of V and T, $K_D[V, T]$ for given material parameters.

Results

Figure 3 shows calculated K_D, where σ_{Y0}=300MPa, n=5 and r_c=0.3mm. Process zone size for a propagating crack has not been examined in detail yet. The authors examined a distribution of tear-ridges behind the tip of a crack arrested in a CTOD test specimen of HT50 steel. The tear-ridges were observed as far as 1mm behind the crack-tip. It is not unreasonable, therefore, to assume r_c value of an order of 0.1 to 1mm. Also, σ_F value was determined so that realistic K_D value was obtained (see below for more detail). Under a constant temperature, K_D once decreases, shows a minimum and then increases with V. The initial decrease is due to the increased strain-rate and elevated yield stress. The increase at high V is due to the reduced stress singularity. K_D diverges at a certain crack velocity, which coincides with c_R calculated using E_t instead of E. With increasing temperature, equivalent strain at $r=r_c$ increases for compensating lower initial yield stress with increased strain-hardening, thereby decreasing instantaneous strain-hardening rate. Therefore, the upper limit crack velocity decreases with increasing temperature. Although theoretical upper limit crack velocity in elastic solid is c_R [2] (2950m/s for E=200GPa and n=0.3), that obtained in experiments is much lower than c_R [1]. This is because of the plastic deformation at the crack-tip. Trend that the calculated upper limit crack velocity decreases with increasing temperature compares well with experiment [1]. Only a slight decrease in σ_F, from 4200MPa to 4000MPa, produced considerably large decrease in K_D; equivalent temperature shift is approximately 20deg.C.

EXTENDED MODEL (SIMULATION OF CRACK PROPAGATION AND ARREST)

Theory

Figure 4 shows configuration of a typical double tension test specimen. Temperature distribution, T[x], is given in the specimen width direction, x. The crack initiated at sub-loading part propagates, enters into the higher temperature region and is finally arrested. The present extended model simulates the crack propagation and arrest behavior in this kind of the test. Figure 5 schematically shows a fracture surface. Because of low stress-triaxiality near the plate surfaces, brittle fracture does not take place there; unbroken

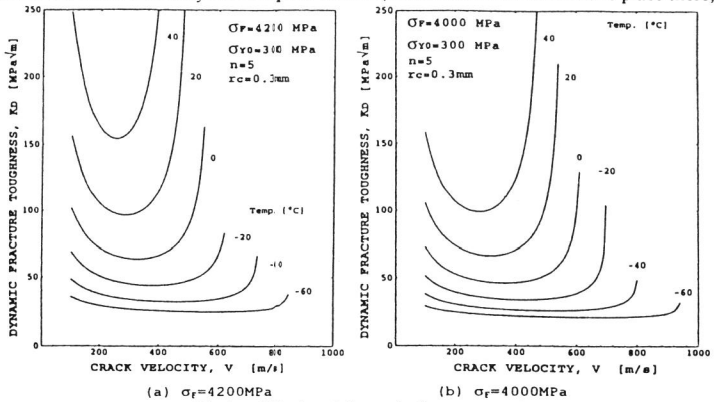

(a) σ_F=4200MPa (b) σ_F=4000MPa

Fig.3—Calculated dynamic fracture toughness.

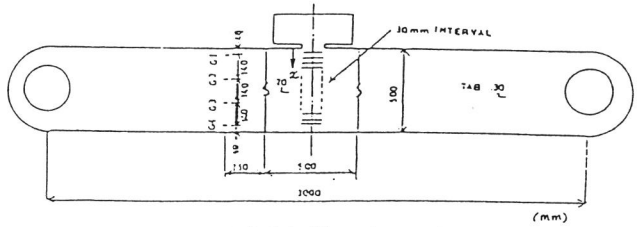

FIG.4—Typical double tention specimen

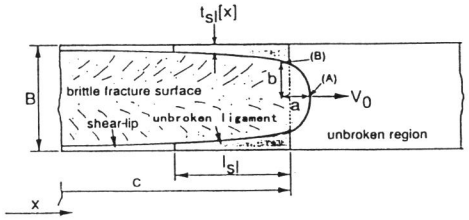

FIG.5—Fracture surface of a propagating crack, schematic

ligaments (UL) are formed. Because the UL receives plastic deformation with crack advancement, tensile stress approximately equal to yield stress acts on it. The UL is plastically elongated and finally fractures in ductile manner; the shear-lips form. Inside the shear-lips, there exists

Brittle crack front bows out in the middle of the plate thickness. At each point along the crack front, there is a pair of the values of dynamic stress intensity factor and crack velocity normal to the crack front. Fundamentally, the pair of these values is assumed to lie on the K_D[V,T] curve determined in the fundamental model. In the extended model, however, the crack front shape is assumed to be semi-elliptical, for simplicity, and the above assumption is assumed to hold only at mid-thickness point, (A), and nearest-the-surface point, (B). At point (A), normal crack velocity is equal to macroscopic crack velocity, V_0. Although normal crack velocity at point (B) is mathematically zero, a brittle crack cannot propagate in steel at very low speed [1]. Here, we assume that lower limit crack velocity, V_{min}, is assumed to exists, which cannot be determined from the present model and is assumed to be 100m/s, tentatively. From the balance between K_d and K_D at point (A) and (B), we obtain,

$$K_{d(A)} = K_D[V_0, T[x]] \tag{8}$$

$$K_{d(B)} = K_D[V_{min}, T[x]] \tag{9}$$

where $K_{d(A)}$ and $K_{d(B)}$ are dynamic stress intensity factors at point (A) and (B), respectively.

Plastic zone size corresponding to $K_{d(B)}$ is calculated as,

$$r_p = \frac{1}{6\pi}\left(\frac{K_{d(B)}}{\sigma_Y}\right)^2 \tag{10}$$

As a point approaches from the mid-thickness point (z=0) to plate surface (z=B/2), stress triaxiality decreases. Weiss and Senguputa [11] showed that thickness of the region where the stress triaxiality falls from that of the plane-strain condition is proportional to r_p. It is assumed that brittle fracture cannot take place within this region; the UL is formed. Therefore, the UL thickness, t_{sl}, is simply expressed as,

$$t_{sl} = k_{sl}\ r_p \tag{11}$$

where, we set the value of the proportionality factor, k_{sl}, as 2, referring to Weiss and Senguputa's result, and r_p is expressed by Eq.(10). Because $K_{d(B)}$ (Eq.(9)) and σ_Y (a constant strain-rate, $10^3 s^{-1}$, in the UL is assumed for simplicity) are expressed as functions of T[x], t_{sl} is also a function of T[x] and therefore a function of x and does not depend on V_0 in the present model.

The above aspects of the crack propagation are difficult to formulate as fully three-dimensional. Here, the model is simplified into the two-dimensional model.

The effect of the UL is represented by crack-closure stress, σ_{sl}[x], imposed on the crack faces behind the crack-tip, see Fig.6. Stress acting on the UL is assumed to be equal to σ_Y and t_{sl}[x] is averaged in the thickness direction, i.e.

$$\sigma_{sl} = \sigma_Y \frac{2\,t_{sl}}{B} \tag{12}$$

where, B is plate thickness.

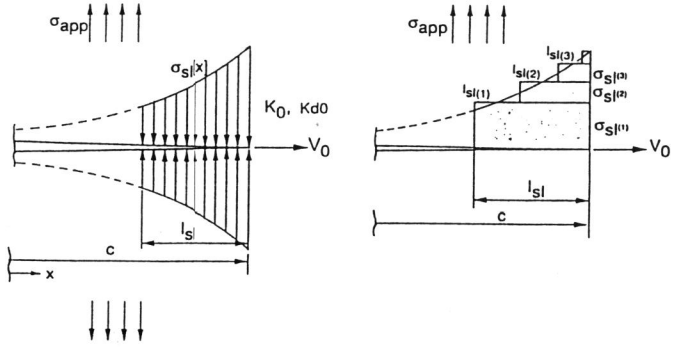

FIG.6—Two dimensional modeling of a propagating crack

Dynamic stress intensity factor for a crack of length 2c with constant remote stress, σ_{app}, and a constant crack-closure stress, σ_{sl}, over a length l_s behind the crack-tip is expressed as [12],

$$K_{d0} = f_K[V_0]K_0 = f_K[V_0]\sigma_{app}\sqrt{\pi c}\left\{1 - \frac{2}{\pi}\frac{\sigma_{sl}}{\sigma_{app}}\cos^{-1}\left[\frac{c - l_{sl}}{c}\right]\right\} \tag{13}$$

where, K_0 is static stress intensity factor, $f_K[V_0]$ is ratio of dynamic to static stress intensity factors and a function of V_0 [2]. Non-uniform crack-closure stress, $\sigma_{sl}[x]$, is discretized into constant crack-closure stresses and Eq.(13) is superimposed for each discretized crack-closure stress (see Fig.6-(b)). It should be mentioned that Eq.(13) is valid for infinite plate with constant σ_{app}. In the real specimen, however, the specimen width is finite and also load drop may take place during crack propagation. Influence of the finite width may be neglected for not too large crack length to width ratio. Also, in a specimen with large pin-to-pin length to the width ratio, e.g. larger than 3, all the crack propagation process is expected to finish before the stress wave reflected at the pin comes back to the center of the specimen. In this case, the influence of the load drop can be neglected.

The UL receives 45 degree slip deformation and finally fractures in shear, see Fig.7. Therefore, the critical opening displacement for the ductile shear fracture of the UL is expressed as,

$$2u_y[c - l_{sl}] = k_s \quad t_{sl}[c - l_{sl}]\varepsilon_F \tag{14}$$

where, $u_y[x]$ is crack opening displacement as a function of x, the left hand side of the equation is crack opening displacement at the end point of the UL, i.e. $x=c-l_{sl}$, k_s is a constant and assumed to be equal to unity, and e_F is critical strain for ductile fracture. $u_y[x]$ was obtained by [13].

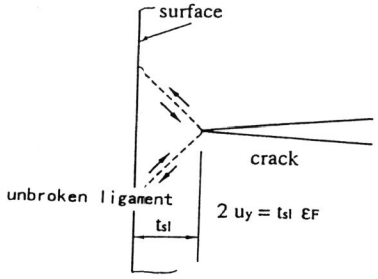

FIG.7 Plastic deformation at the unbroken ligament, cross section

Results

Part of the present authors previously conducted a series of double tension tests [14], which are computer-simulated by the present model. The steels tested are two kinds of 20mm thick mild steels, steel-A and steel-E, for ship structures with practically the same yield strength, approximately 300MPa, and different temperature distribution, arrest crack length, c_a, was changed. Arrest toughness, K_{ca}, is empirically calculated from σ_{app} and c_a by using the tangent formula [15],

$$K_{ca} = \sigma_{app}\sqrt{2W \tan[\pi c_a / 2W]} \tag{21}$$

Figures 8-(a) and (b) show observed histories of V_0 measured by crack-detector gages for steel-A and steel-E, respectively.

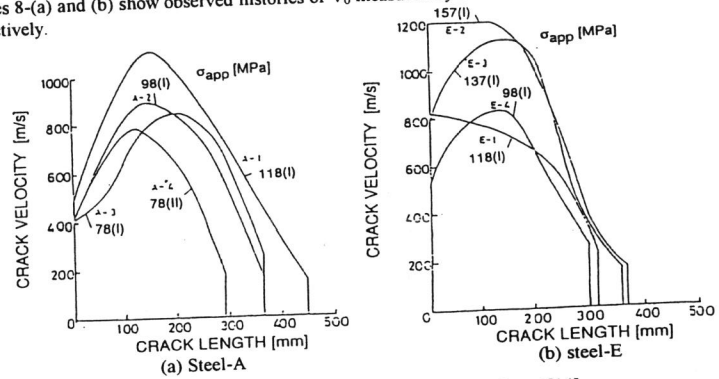

(a) Steel-A (b) steel-E

FIG.8--History of crack velocity, experiment[14].

In the simulation, we use the same values of material parameters shown in Fig.3. In addition, we set e_F =0.1. Values of σ_F for the both steels were determined so that the calculated ca for the lowest σ_{app} roughly agreed with the experiments: σ_F=4000MPa for steel -A and 4200MPa for steel-E.

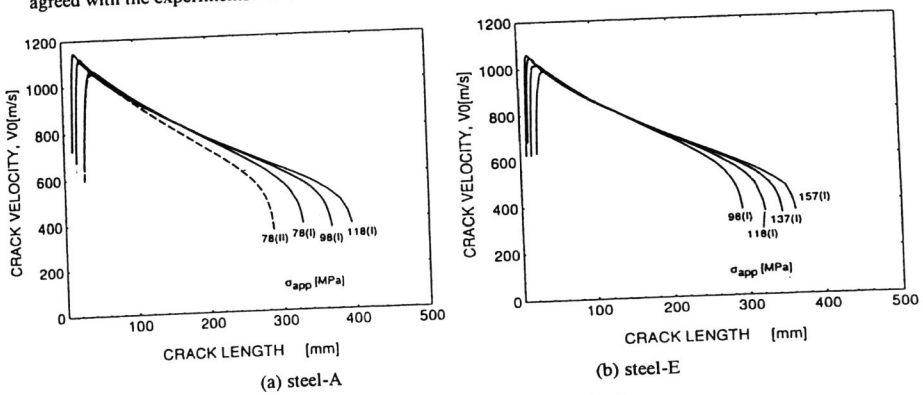

(a) steel-A (b) steel-E

FIG.9--Caclulated history of crack velocity.

Figures 9-(a) and (b) show calculated histories of V_0. V_0 increases steeply just after crack initiation,

attains a maximum, decreases and the crack is finally arrested. Although there is a discrepancy at the very initial stage of the crack propagation, calculated histories of V_0 well compare with the experiment.

Figure 10 shows measured and calculated K_{ca} for the two steels. Considering the possible deviation of temperature distribution from the target, the calculated K_{ca} compare well with the measured K_{ca}. Although a parameter which depends on temperature is yield stress only in the present model, calculated temperature dependency of K_{ca} are well reproduced.

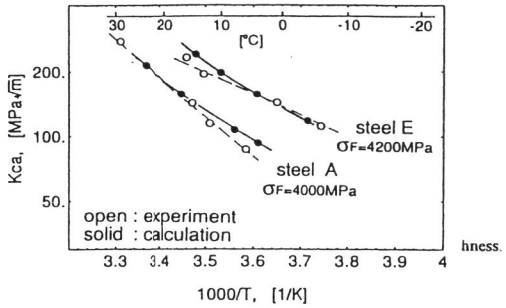

FIG.10--Comparison between calculated and experimental arrest toughness.

Unfortunately, record of the fracture surfaces in the experiment is not available. Thus, we refer to the fracture surface observations by Akita et al. [16] for different series of the temperature-gradient type ESSO tests and compare them with the present calculation, only qualitatively. Figure 11 is a redrawing from the fracture surface photographs [16]. Only the arrest crack-tip region is shown and the actual arrest crack length changed with σ_{app}. With increasing σ_{app} and increasing arrest temperature, thickness of the UL at crack arrest increased (distinction between UL and shear-lip is impossible) and the crack front bowing became more pronounced. This tendency compares well with the calculation shown in Fig. 12.

Figure 12 also shows that the crack front shape during propagation is straighter for lower temperature and higher V_0. This tendency has been observed empirically but no explanation has been made. At low temperature, K_D depends on V weakly except near the upper limit velocity. In addition, V_0 tends to be high at low temperature, closer to the upper limit velocity. At this circumstance, $K_{D(A)}$ tends to be larger than $K_{D(B)}$. Because K_d is equal to K_D at both points, crack front shape becomes straighter so that $K_{d(A)}$ is larger than

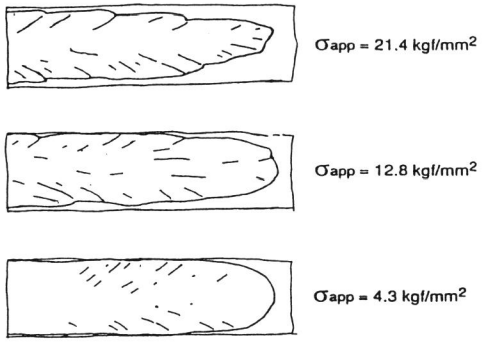

FIG.11 Fracture surface profiles, redrawing from [16]

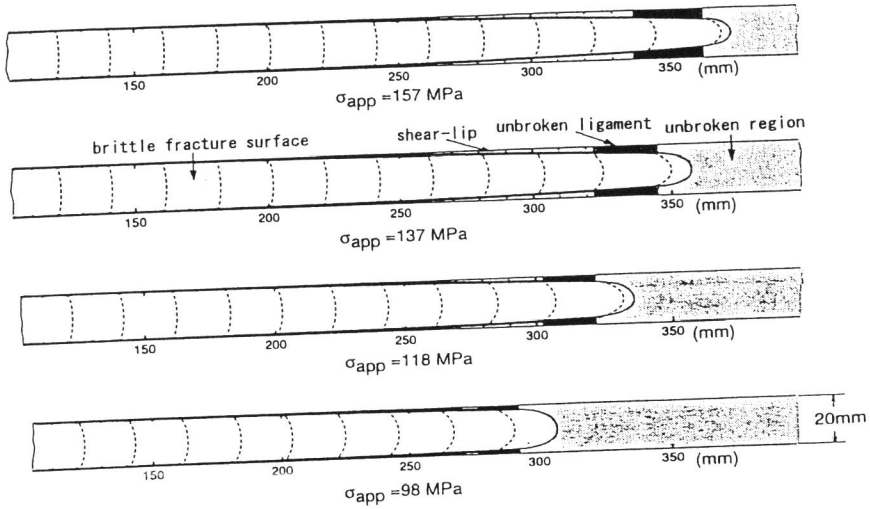

FIG.12--Calculated fracture surface profiles, steel-E.

$K_{d(B)}$. Conversely, $K_{D(A)}$ tends to be lower than $K_{D(B)}$ at high temperature and low V_0, and the crack front bowing becomes more pronounced (right side of the Figure). Even at low temperature, crack front bowing becomes pronounced at low crack velocity, especially just before crack arrest. Figure 13 shows change of $K_{d(A)}$ with V_0 for steel-E. $K_D[V,T]$ curves are also plotted. After accelerated at low temperature, the crack is decelerated, while $K_{d(A)}$ increases. In turn, $K_{d(A)}$ begins to decrease with K_d continuing to increase. This is due to the double effects mentioned above. At the minimum $K_D[V,T]$ point, it becomes no longer possible to maintain the equality between $K_{d(A)}$ and $K_D[V,T]$; the former tends to decrease and the latter tends to increase and the crack is arrested. The crack is not arrested with V_0 continuously decreasing down to zero, but there is a lower limit. Calculated lower limit V_0 ranges from 300 to 350m/s and measured lower limit V_0 ranges from 200 to 300m/s (Fig.13). Considering the difficulty in measuring the

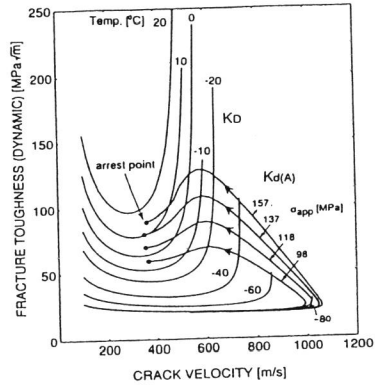

FIG.13--History of dynamic stress intensity factor and crack velocity at mid-thickness point, steel-E.

crack velocity and its accuracy, especially just before crack arrest, the present model reproduces the crack arrest behavior well. It should be emphasized here that the lower limit crack velocity assumed in Eq.(9) is the *local* lower limit crack velocity and is not the same as the *macroscopic* lower limit crack velocity discussed here.

Figure 14 shows a comparison between K_{ca} with UL, K_{ca} without UL (t_{sl}=0.1mm). K_{ca}(without UL) is considered to be plane-strain arrest toughness. Minimum K_D at each temperature (Fig.3) is plotted for reference. Note that Eq.(21) is not used for calculating K_{ca} but the formula for an infinite plate is used, instead. Difference between K_{ca}(with UL) and K_{ca}(without UL) are significantly large, especially at high temperature. Temperature dependence of K_{ca}(without UL) is milder than that of K_{ca}(with UL) and that of measured K_{ca}. It is indispensable to take account of the effect of the UL for predicting the actual temperature dependence of the arrest toughness.

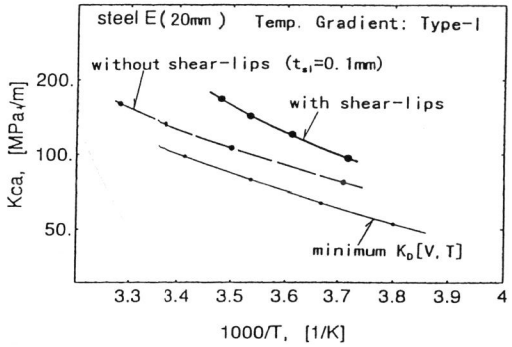

FIG.14 Calculated influence of UL on arrest toughness, steel-E

DISCUSSION

It has been shown that the present model reproduces actual crack propagation and arrest behavior well. Considering the possible experimental errors, the present model predicts arrest crack length and arrest toughness with a reasonable accuracy.

σ_F was determined so that calculated arrest crack length agreed with the measured value at a certain experimental condition. At this moment, however, it is impossible to determine σ_F value experimentally. The assumed value of σ_F is rather high as compared with σ_F of brittle cleavage crack initiation in steel [17]. While brittle micro phase has a significant influence on cleavage crack initiation, its effect is not so significant for crack propagation [18]. In addition, tear-ridges are formed on the propagating crack surface. The tear-ridges connect the crack faces behind the crack-tip and may have the crack-closure effect in the microscopic level. These factors may justify the assumed high value of σ_F for crack propagation.

Importance of the UL has been pointed out in the present model. Even with the same K_D[V,T] values, K_{ca} can be varied by a change in the UL formation. Hence, the effect of the temperature-gradient was studied. Temperature-gradient for the standard (W=0.5m) and wide plate (W=2.0m) specimen was changed, while the temperatures at both sides were kept unchanged, T_0=-90deg.C and T_1=50deg.C. Figure 15 shows calculated apparent arrest toughness, K_{ca}. Higher K_{ca} value for the wide plate specimen (mild temperature- gradient) than that for the standard specimen (steep temperature- gradient) is obtained. This means that K_{ca} is not a unique material parameter describing the arrest resistance of steel, but depends on temperature-gradient. Although the change in K_{ca} becomes larger with larger value of assumed σ_F, it is not very significant. It should be mentioned that K_{ca} obtained from a specimen with steep temperature-gradient is a lower bound value and may be regarded as a conservative estimation [19].

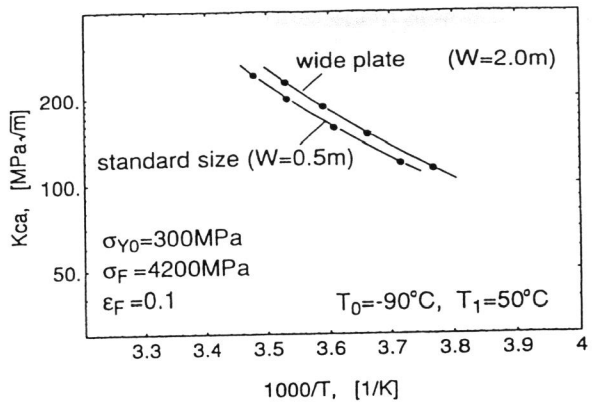

FIG.15--Calculated influence of temperature-gradient on arrest toughness.

For a tough material, it is sometimes difficult to obtain plane-strain arrest toughness. Side-grooves may be applied to suppress the formation of the UL or shear-lips [20]. If the effect of the UL is estimated accurately, plane-strain arrest toughness may be predicted from the arrest test accompanying the UL based on the present theory. This is subject to a future work.

CONCLUSIONS

(1) Dynamic fracture toughness, K_D, is calculated from fundamental material parameters based on the local fracture stress criterion. K_D is expressed as a function of crack velocity and temperature.
(2) K_D has a minimum with respect to crack velocity and diverges at an upper limit crack velocity, which is related to the Rayleigh wave speed for plastic deformation and decreases with increasing temperature.
(3) A model is proposed which takes account of the unbroken-ligament formed near the plate surface and of the crack-front-bowing in the middle of the plate thickness. The model simulates crack propagation and arrest behavior in a specimen with temperature-gradient. By assuming a suitable value of local fracture stress, calculated arrest length and apparent arrest toughness agree well with experiment.
(4) The effect of the unbroken-ligament is significant in suppressing the crack propagation. It changes with temperature-gradient. Arrest toughness calculated from applied stress and arrest crack length is not a unique material parameter but depends on the temperature-gradient, although weakly.

REFERENCES

[1] Kanazawa, T., Machida, S., Teramoto, T. and Yoshinari, H., "Study on Fast Fracture and Crack Arrest", Experimental Mechanics, Feb. 1981, pp 79-88.
[2] Freund, L. B., Dynamic Fracture Mechanics, Cambridge University Press, 1990.
[3] Machida, S. Yoshinari, H., Yasuda, M., Aihara, S. and Mabuchi, H., "Fracture Mechanical Modeling of Brittle Crack Propagation and Arrest of Steel", Proceedings of the 1995 Joint ASME/JSME Pressure Vessels and Piping Conference, PVP-vol.300, p 183-195, ASME, 1995.
[4] Ritchie, R. O., Knott, J. F. and Rice, J. R., "On the Relationship between Critical tensile Stress and Fracture Toughness in Mild Steel", J. Mechanics and Physics of Solids, vol.21, 1973, pp 395-410.
[5] Miyata, T., Ohtsuka, A., Mitsubayashi, M., Haze, T. and Aihara, S., "Prediction of Fracture Toughness by Local Fracture Criterion", ASTM STP 1074, 1990, p 361-377.
[6] Achenbach, J. D., Kanninen, M. F. and Popelar, C. H., "Crack-Tip Fields for Fast Fracture of an Elastic-Plastic Materials", J. Mechanics and Physics of Solids, vol.29, 1981, pp 211-225.
[7] Hutchinson, J. W., "Singular Behaviour at the End of a Tensile Crack in a Hardening Material", J.

Mechanics and Physics of Solids, vol.16, 1968, pp 13-31.
[8] Amazigo, J. C. and Hutchinson, J. W., "Crack-Tip Fields in Steady Crack-Growth with Linear Strain-Hardening", J. Mechanics and Physics of Solids, vol.25, 1977, pp 81-97.
[9] Sundararajan, G. and Shewmon, P. G., "The Use of Dynamic Impact Experiments in the Determination of the Strain Rate Sensitivity of Metals and Alloys", Acta Metallurgica, vol.31, 1983, pp 101-109.
[10] Campbell, J. D. and Ferguson, W. G., "The Temperature and Strain-Rate Dependence on the Shear Strength of Mild Steel", Philosophical Magazine, vol.21, 1970, pp 63-82.
[11] Weiss, V. and Senguputa, M., "Ductility, Fracture Resistance and R-Curves", ASTM STP 590, 1976, p 194-207.
[12] Freund, L. B., "Crack Propagation in an Elastic Solid Subjected to General Loading -II, Non Uniform Rate of Extension", J. Mechanics and Physics of Solids, vol.20, 1972, pp 141-152.
[13] Embley, G. T. and Sih, G. C., "Plastic Flow Around an Expanding Crack", Engineering Fracture Mechanics, vol.4, 1972, pp 431-442.
[14] Kanazawa, T., Machida, S., Teramoto, T., Yoshinari, H. and Miyahara, T., "Study on Fast Fracture and Crack Arrest (5th Report)", Journal of Society of Naval Architects of Japan, vol.150, 1981, p 504-510.
[15] Tada, H., Paris, P. C. and Irwin, G. R., Stress Analysis of Cracks Handbook, Hellertown: Del research Corporation, 1973.
[16] Akita, Y. and Ikeda, K., "On the Brittle Crack Propagation and Arrest with Special Reference to ESSO Test with Temperature Gradient", Journal of Society of Naval Architects of Japan, vol.112, 1962, p 153-162.
[17] Bowen, P., Druce, S. G. and Knott, J. F., "Effects of Microstructure on Cleavage Fracture in Pressure Vessel Steel", Acta Metallurgica, vol.34, 1986, pp 1121-1131.
[18] Aihara, S., "Influence of HAZ Microstructure on Brittle Fracture Initiation and Arrest Toughness", CAMP-ISIJ, vol.7, 1994, p.843.
[19] Mimura, H., "Method to Estimate Kca from K1a", J. High Pressure Institute, Japan, vol.31, 1993, pp 58-64.
[20] ASTM E 1221-88, "Standard Test Method for Determining Plane-Strain Crack-Arrest Fracture Toughness, Kia, of Ferritic Steels", 1988.